# Graviton-induced bremsstrahlung

Erik Dvergsnes* and Per Osland†
*Department of Physics, University of Bergen, Allégaten 55, N-5007 Bergen, Norway*

Nurcan Öztürk‡
*Department of Physics, University of Bergen, Allégaten 55, N-5007 Bergen, Norway*
*and Department of Physics, University of Texas, Arlington, Texas 76019*
(Received 22 July 2002; published 10 April 2003)

We discuss photon bremsstrahlung induced by virtual graviton exchange in proton-proton interactions at hadronic colliders, resulting from the exchange of Kaluza-Klein excitations of the graviton. The relevant subprocesses $gg \to G \to e^+e^-\gamma$ and $q\bar{q} \to e^+e^-\gamma$ are discussed in both the Arkani-Hamed–Dimopoulos–Dvali and the Randall-Sundrum scenarios. Although two-body final states (or real graviton emission) would presumably be the main discovery channels, a search for three-body final states could be worthwhile since such events have characteristic features that could provide additional confirmation. In particular, the $k_\perp$ distribution of the photon is in both scenarios harder than that of the standard-model background.

DOI: 10.1103/PhysRevD.67.074003 PACS number(s): 13.85.−t, 04.50.+h, 12.60.−i

## I. INTRODUCTION

The idea of additional compact dimensions and strings at the TeV scale, proposed by Antoniadis [1] for solving the hierarchy problem, together with the idea that standard-model (SM) fields live on branes in a higher-dimensional space [2] have led to the even more radical speculations that extra dimensions might be macroscopic, with SM fields confined to the familiar four-dimensional world (brane) [3,4]. The models which allow for gravity effects at the TeV scale can be grouped into two kinds: those of factorizable geometry, where the extra dimensions are macroscopic [3] [Arkani-Hamed–Dimopoulos–Dvali (ADD) scenario], and those of non-factorizable (warped) geometry, the simplest example of which has only one extra dimension separating ''our'' brane from a hidden brane [4] [Randall-Sundrum (RS) scenario].

In both these scenarios, the propagation of gravitons in the extra dimensions leads to gravitons which from the four-dimensional point of view are massive. In the ADD scenario, these Kaluza-Klein (KK) gravitons have masses starting at values of the order of meV, and there is practically a continuum of them, up to some cutoff $M_S$ (close to the effective Planck scale) of the order of TeV, whereas in the RS scenario they are widely separated resonances with mass splittings of the order of TeV. In both cases, they have a universal coupling to matter and photons via the energy-momentum tensor.

These recent speculations have led to several studies [5–13] of various experimental signals induced by graviton production and exchange. The new scenarios allow for the emission of massive gravitons [5–7], which would lead to events with missing energy (or transverse momentum), as well as effects due to the exchange of virtual gravitons (in addition to photons and $Z$'s) [5,7,8,11]. These processes include the production of dileptons and diphotons in electron-positron collisions, as well as gluon-gluon and quark-antiquark-induced processes at the Fermilab Tevatron and CERN Large Hadron Collider (LHC).

In fact, several searches at the CERN $e^+e^-$ collider LEP and the Tevatron have given direct bounds on the effective Planck scale, of the order of a TeV [13–15], while astrophysical arguments result in very strong limits when applied to the simplest ADD scenarios, for $n=2$ and 3 extra dimensions [16]. Of course, the direct experimental searches are most worthwhile. The above studies all focus on two-body final states, which are expected to be dominant, and therefore lead to the most stringent bounds on the existence of extra dimensions.

Here we shall investigate photon bremsstrahlung induced by graviton exchange [17]. While this cross section is further reduced by $\mathcal{O}(\alpha/\pi)$, so is the background. It has some characteristic features resulting from the exchange of a spin-2 particle and from the direct graviton-photon coupling that we would like to point out. These features may be useful in discriminating any signal against the background.

Specifically, we shall consider the process

$$pp \to e^+e^-\gamma + X, \tag{1.1}$$

which may get a contribution due to graviton exchange, and which for energetic electrons (or muons) and photons should experimentally be a very clean signal. (There is also a related process, where a graviton is emitted in the final state [18].)

Since this final state is very distinct, and since the standard-model (Drell-Yan) background is well understood, the process (1.1) may offer some hope for observing a signal or improving on the exclusion bounds.

This paper is organized as follows: First (Sec. II) we consider the gluon-gluon fusion contribution to both two-body and three-body final states. Then (Sec. III) we consider quark-antiquark annihilation, which also gives rise to the standard-model background. We calculate the cross section by summing over the KK tower within the ADD (Sec. IV) and RS (Sec. V) scenarios for a selected choice of parameters, and finally we give some concluding remarks (Sec. VI).

*Email address: erik.dvergsnes@fi.uib.no
†Email address: per.osland@fi.uib.no
‡Email address: nurcan@uta.edu

 

## II. GLUON-GLUON FUSION

We shall first discuss gluon-gluon fusion. Because of the increasing gluon luminosity at high energies (LHC), this contribution will be dominant for a certain range in invariant mass of the (three-body) final state. At even higher invariant masses, the contribution to the signal, from quark-antiquark annihilation, becomes dominant.

### A. Two-body final states

The process of interest, Eq. (1.1), is related to the two-body final state

$$pp \to e^+e^- + X, \tag{2.1}$$

which may proceed via gluon-gluon fusion and an intermediate graviton,

$$gg \to G \to e^+e^-. \tag{2.2}$$

For massless electrons, the cross section for single graviton exchange resulting from gluon-gluon fusion is (in agreement with the results of [12])

$$\hat{\sigma}^{(G)}_{gg\to ee} = \frac{\kappa^4 \hat{s}}{10240\pi} \frac{\hat{s}^2}{(\hat{s}-m_{\vec{n}}^2)^2 + (m_{\vec{n}}\Gamma_{\vec{n}})^2}, \tag{2.3}$$

with $\hat{s} = (k_1+k_2)^2$ the two-gluon invariant mass squared. Furthermore, $m_{\vec{n}}$ and $\Gamma_{\vec{n}}$ are the mass and width of the graviton,[1] and $\kappa$ is the graviton coupling, to be defined below. The angular distribution, which is forward-backward symmetric, is given by $1-\cos^4\theta$, where $\theta$ is the c.m. scattering angle.

With $\xi_1$ and $\xi_2$ the fractional momenta of the two gluons, $k_1 = \xi_1 P_1$, $k_2 = \xi_2 P_2$, and $P_1$ and $P_2$ the proton momenta, $(P_1+P_2)^2 = s$, we have $\hat{s} \simeq \xi_1\xi_2 s$. For the overall process (2.1) we thus find the differential cross section

$$\begin{aligned}\frac{d\sigma^{(G)}_{gg\to ee}}{d\hat{s}} &= \int_0^1 d\xi_1 \int_0^1 d\xi_2 \; f_g(\xi_1) f_g(\xi_2) \; \frac{d\hat{\sigma}^{(G)}_{gg\to ee}}{d\hat{s}} \\ &= \int_0^1 d\xi_1 \int_0^1 d\xi_2 \;\; f_g(\xi_1) f_g(\xi_2) \\ &\quad \times \delta(\xi_1\xi_2 s - \hat{s}) \;\; \hat{\sigma}^{(G)}_{gg\to ee}(\hat{s}) \\ &= \frac{1}{s} I_{gg}(\hat{s}) \;\; \hat{\sigma}^{(G)}_{gg\to ee}(\hat{s}),\end{aligned} \tag{2.4}$$

with the relevant convolution integral, $I_{gg}(\hat{s})$, over the gluon distribution functions given by Eq. (A1) in Appendix A.

[1]The Kaluza-Klein index, $\vec{n}$ on $m_{\vec{n}}$ and $\Gamma_{\vec{n}}$ should not be confused with $n$, the number of extra dimensions.

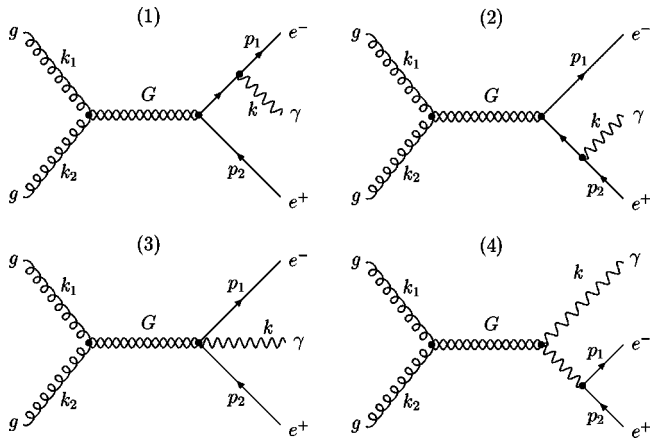


FIG. 1. Feynman diagrams for $gg \to G \to e^+e^-\gamma$. [There is a corresponding set of diagrams with $q\bar{q}$ initial states, which we shall refer to as "set *B*." The SM diagrams corresponding to diagrams (1) and (2), with $q\bar{q}$ initial states and a photon or $Z$ instead of the graviton, will be referred to as "set $D_\gamma$" and "set $D_Z$."]

### B. Three-body final states

Let us now consider the contribution from gluon-gluon fusion to the bremsstrahlung process in Eq. (1.1). The underlying subprocess

$$gg \to G \to e^+e^-\gamma, \tag{2.5}$$

can proceed via the four Feynman diagrams of Fig. 1, the basic couplings for which are given by Han *et al.* [7] (see also Giudice *et al.* [5]).

The evaluation of the cross section is straightforward, and the differential cross section (with respect to the azimuthal angle, $\chi$, and $\cos\theta$, where $\theta$ is the angle between the photon and the beam) is of fourth order in the invariants. This is due to the underlying mechanism being the exchange of a spin-2 object. It is straightforward to verify that it is gauge invariant with respect to the gluons, as well as to the photon (actually, diagram 4 is by itself gauge invariant). But the expression is quite lengthy, so we shall not write it out here.

The angular distribution of the (two-body) non-radiative cross section (2.3) is given by fourth-order polynomials in $\cos\theta$. Here, just like in gluon bremsstrahlung (see, e.g., [19]), there is an accompanying dependence on the azimuthal angle $\chi$, but now up to fourth order in $\cos\chi$, or, equivalently, up to $\cos 4\chi$.

After integrating over the azimuthal orientation of the events, the cross section is of the form

$$\begin{aligned}\frac{d^3\hat{\sigma}^{(G)}_{gg\to ee\gamma}}{dx_1 dx_2 d\cos\theta} &\sim b_0(x_1,x_2) + b_2(x_1,x_2)\cos^2\theta \\ &\quad + b_4(x_1,x_2)\cos^4\theta,\end{aligned} \tag{2.6}$$

similar to the two-body final states, i.e., the gluon-gluon fusion does not contribute to any forward-backward asymmetry.

In our calculations we have chosen the unitary gauge ($\xi^{-1}=0$ in the notation of [7]), whereby the scalar exchange

decouples. After averaging and summing over gluon, electron and photon polarizations, and integrating over event orientations with respect to the gluon momentum, we find (for exchange of a single graviton)

$$\frac{d^2\hat{\sigma}^{(G)}_{gg\to ee\gamma}}{dx_1 dx_2} = \frac{\alpha\kappa^4 \hat{s} Q_e^2}{2560\pi^2} \frac{\hat{s}^2}{(\hat{s}-m_{\tilde{n}}^2)^2+(m_{\tilde{n}}\Gamma_{\tilde{n}})^2} X_B(x_1,x_2), \tag{2.7}$$

with $X_B(x_1,x_2)$ given by Eq. (A8) in Appendix A. Furthermore, $\alpha$ is the fine-structure constant, $Q_e=-1$ is the electron charge, and $x_1$, $x_2$ and $x_3$ denote the fractional energies of the electrons and the photon in the c.m. frame,

$$x_1 = E_1/\sqrt{\hat{s}}, \quad x_2 = E_2/\sqrt{\hat{s}}, \qquad x_3 = \omega/\sqrt{\hat{s}}, \quad 0 \leqslant x_i \leqslant \frac{1}{2}, \tag{2.8}$$

with $x_1+x_2+x_3=1$. The expression $X_B(x_1,x_2)$ exhibits the familiar singularities in the infrared and collinear limits, $s_1 \equiv (p_1+k)^2 = \hat{s}(1-2x_2) \to 0$, and $s_2 \equiv (p_2+k)^2 = \hat{s}(1-2x_1) \to 0$, as well as a collinear singularity at $s_3 \equiv (p_1+p_2)^2 = \hat{s}(1-2x_3) \to 0$ due to the fourth Feynman diagram. Here $\hat{s} \equiv (k_1+k_2)^2 = (p_1+p_2+k)^2$. The additional singularity means that there is a tendency to have events with hard photons [17]. This is one way in which these events differ from ordinary QED-based bremsstrahlung.

The differential cross section in Eq. (2.7) can be written more compactly as

$$\frac{1}{\hat{\sigma}^{(G)}_{gg\to ee}} \frac{d^2\hat{\sigma}^{(G)}_{gg\to ee\gamma}}{dx_1 dx_2} = \frac{4\alpha Q_e^2}{\pi} X_B(x_1,x_2), \tag{2.9}$$

with $\hat{\sigma}^{(G)}_{gg\to ee}$ given by Eq. (2.3). As we see, the cross section is reduced by a factor $\mathcal{O}(\alpha/\pi)$ compared to the two-body cross section.

Analogous to Eq. (2.4), we find for the gluon contribution to the overall process (1.1)

$$\frac{d^3\sigma^{(G)}_{gg\to ee\gamma}}{d\hat{s}\,dx_1 dx_2} = \frac{1}{s} I_{gg}(\hat{s}) \frac{d^2\hat{\sigma}^{(G)}_{gg\to ee\gamma}}{dx_1 dx_2}, \tag{2.10}$$

with the convolution integral given by Eq. (A1) in Appendix A.

## III. QUARK-ANTIQUARK ANNIHILATION

Another process which contributes to Eq. (1.1), and gives rise to the SM background, is quark-antiquark annihilation. Furthermore, at large invariant masses of the final state, it also gives the most important contribution to the signal.

### A. Two-body final states

The process in Eq. (2.1) may also proceed via quark-antiquark annihilation and an intermediate graviton, with the following cross section for single graviton exchange (initial state quarks are considered massless):

$$\hat{\sigma}^{(G)}_{q\bar{q}\to ee} = \frac{\kappa^4\ \hat{s}}{15360\pi} \frac{\hat{s}^2}{(\hat{s}-m_{\tilde{n}}^2)^2+m_{\tilde{n}}^2\Gamma_{\tilde{n}}^2}, \tag{3.1}$$

in agreement with [5,12]. It differs from the cross section for gluon-gluon fusion by a factor 2/3.

There is also a SM background to this process, where the same final state is produced through photon or $Z$ exchange. This well-known cross section is given by

$$\hat{\sigma}^{(\mathrm{SM})}_{q\bar{q}\to ee}(\hat{s}) = \frac{4\pi\alpha^2}{9\hat{s}}[Q_q^2\ Q_e^2 + 2Q_q Q_e v_q v_e\ \mathrm{Re}\,\chi(\hat{s}) + (v_q^2+a_q^2)(v_e^2+a_e^2)|\chi(\hat{s})|^2], \tag{3.2}$$

with

$$\chi(\hat{s}) = \frac{1}{\sin^2(2\theta_W)} \frac{\hat{s}}{(\hat{s}-m_Z^2)+im_Z\Gamma_Z}, \tag{3.3}$$

where we have normalized vector and axial-vector couplings to $v_f = T_f - 2Q_f \sin^2\theta_W$ and $a_f = T_f$, respectively, with $T_f$ the isospin. Furthermore, $m_Z$ and $\Gamma_Z$ are the mass and width of the $Z$ boson, $Q_q$ the quark charge, and $\theta_W$ the weak mixing angle.

In the case of $q\bar{q}\to G\to e^+e^-$, with the cross section given by Eq. (3.1), the angular distribution is $1-3\cos^2\theta+4\cos^4\theta$, whereas for the photon exchange, Eq. (3.2), the angular distribution is given by the familiar $1+\cos^2\theta$. The interference between graviton and photon exchange has an angular distribution given by $\cos^3\theta$ (as pointed out by Ref. [5]), i.e., *it exhibits a forward-backward asymmetry* and vanishes upon integration. The interference between graviton and $Z$ exchange exhibits a slightly different angular distribution (which also vanishes upon integration).

For $pp$ collisions, we find the graviton contribution to the differential cross section [in accordance with Eq. (2.4)]

$$\frac{d\sigma^{(G)}_{qq\to ee}}{d\hat{s}} = \frac{1}{s} I_{BB}(\hat{s})\ \hat{\sigma}^{(G)}_{qq\to ee}(\hat{s}), \tag{3.4}$$

with $I_{BB}(\hat{s})$ given in Appendix A. The SM contribution can be found in a similar manner, but here the convolution integrals must be weighted by the factors $Q_q^2$, $Q_q v_q$ and $(v_q^2+a_q^2)$ for photon exchange, interference between the photon and the $Z$, and for $Z$ exchange, respectively (see Appendix A). The reason for this is that the convolution integral implicitly contains flavor summation.

### B. Three-body final states

Now we will examine the subprocess

$$q\bar{q}\to e^+e^-\gamma, \tag{3.5}$$

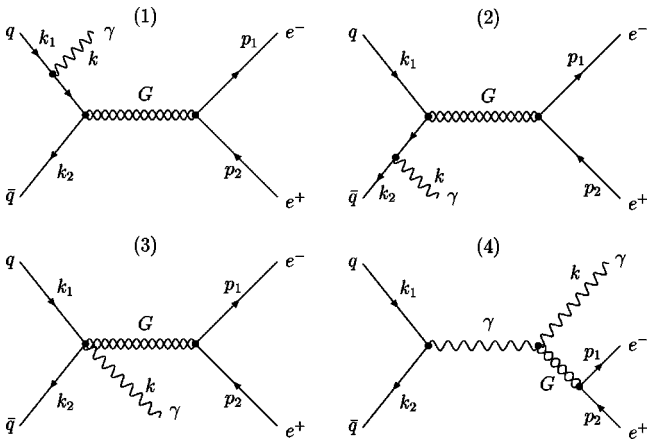


FIG. 2. Feynman diagrams for "initial-state radiation" in $q\bar{q} \to e^+e^-\gamma$. We refer to these diagrams as "set *A*." The SM diagrams corresponding to diagrams (1) and (2), but with a photon or *Z* instead of the graviton, are referred to as "set $C_\gamma$" and "set $C_Z$."

which is determined by four sets of Feynman diagrams. First, there are the diagrams of Fig. 2, referred to as "set *A*," describing "initial-state radiation." Then, there are four diagrams analogous to those of Fig. 1, where the initial-state gluons are replaced by quarks and antiquarks. We shall refer to these as "set *B*;" they describe "final-state radiation." Finally, we have the SM background, which arises from diagrams similar to 1 and 2 of sets *A* and *B*, with a $\gamma$ or *Z* exchanged instead of the graviton. We shall refer to the SM diagrams as "sets $C_\gamma$," "$C_Z$" (initial-state radiation), "$D_\gamma$," and "$D_Z$" (final-state radiation). It is convenient to separate initial- from final-state radiation, since, in the former case, the propagator does not carry all the momentum of the initial quarks.

The $q\bar{q}$-initiated cross section can be decomposed as

$$\hat{\sigma}^{(G)}_{q\bar{q}\to ee\gamma}, \quad \hat{\sigma}^{(\mathrm{SM})}_{q\bar{q}\to ee\gamma}, \quad \hat{\sigma}^{(G,\gamma)}_{q\bar{q}\to ee\gamma}, \quad \text{and} \quad \hat{\sigma}^{(G,Z)}_{q\bar{q}\to ee\gamma}, \tag{3.6}$$

where the first term is the graviton contribution (sets *A* and *B*), the second term is the standard-model background (sets *C* and *D*) and the last two are graviton-photon and graviton-*Z* interference terms, respectively.

First we shall consider the graviton exchange diagrams, where we introduce the following notation:

$$\hat{\sigma}^{(G)}_{q\bar{q}\to ee\gamma} = \hat{\sigma}_A + \hat{\sigma}_B + \hat{\sigma}_{AB}. \tag{3.7}$$

For initial-state radiation (set *A*), we find

$$\frac{d^2\hat{\sigma}_A}{dx_1dx_2} = \frac{\alpha\kappa^4 s_3\, Q_q^2}{12288\pi^2} \frac{s_3^2}{(s_3 - m_{\tilde{n}}^2)^2 + (m_{\tilde{n}}\Gamma_{\tilde{n}})^2} X_A(x_1,x_2), \tag{3.8}$$

where $X_A(x_1,x_2)$ is given by Eq. (A4) in Appendix A. Since the denominator in Eq. (3.8) depends on $s_3 = (1-2x_3)\hat{s}$ instead of $\hat{s}$, this contribution will be smeared out when integrated over $x_3$.

The corresponding result for final-state radiation (set *B*) is

$$\frac{d^2\hat{\sigma}_B}{dx_1dx_2} = \frac{\alpha\kappa^4\hat{s}Q_e^2}{3840\pi^2} \frac{\hat{s}^2}{(\hat{s} - m_{\tilde{n}}^2)^2 + (m_{\tilde{n}}\Gamma_{\tilde{n}})^2} X_B(x_1,x_2), \tag{3.9}$$

with $X_B(x_1,x_2)$ given by Eq. (A8). This contribution is, like in the two-body case, identical to the contribution from gluon-gluon fusion, except for a factor of 2/3.

There is also an interference term, $\hat{\sigma}_{AB}$, between sets *A* and *B*, which has to be considered. It contributes to the forward-backward asymmetry, and vanishes when integrated over all event orientations.

In the three-body case, the SM background becomes

$$\hat{\sigma}^{(\mathrm{SM})}_{q\bar{q}\to ee\gamma} = \hat{\sigma}_C + \hat{\sigma}_D + \hat{\sigma}_{CD}, \tag{3.10}$$

where the contribution of initial- and final-state radiation is given by

$$\frac{d^2\hat{\sigma}_C}{dx_1dx_2} = \frac{3\alpha Q_q^2}{4\pi}\, \hat{\sigma}^{(\mathrm{SM})}_{q\bar{q}\to ee}(s_3) X_C(x_1,x_2),$$
$$\frac{d^2\hat{\sigma}_D}{dx_1dx_2} = \frac{4\alpha Q_e^2}{\pi}\, \hat{\sigma}^{(\mathrm{SM})}_{q\bar{q}\to ee}(\hat{s}) X_D(x_1,x_2), \tag{3.11}$$

with $X_C(x_1,x_2)$ and $X_D(x_1,x_2)$ given in Appendix A, and $\hat{\sigma}^{(\mathrm{SM})}_{q\bar{q}\to ee}$ given by Eq. (3.2). This $\hat{\sigma}_D$ is the familiar bremsstrahlung cross section expressed in terms of the related two-body process. While the contribution of the photon-exchange part of the interference between initial- and final-state radiation to the integrated cross section, $\hat{\sigma}_{C_\gamma D_\gamma}$, vanishes [20], this is not the case for terms involving *Z* exchange [21]. They are included in the full SM background, Eq. (4.8).

For the interference terms between graviton exchange and the SM diagrams, we introduce the following notation:

$$\hat{\sigma}^{(G,\gamma)}_{q\bar{q}\to ee\gamma} = \hat{\sigma}_{AC_\gamma} + \hat{\sigma}_{AD_\gamma} + \hat{\sigma}_{BC_\gamma} + \hat{\sigma}_{BD_\gamma},$$
$$\hat{\sigma}^{(G,Z)}_{q\bar{q}\to ee\gamma} = \hat{\sigma}_{AC_Z} + \hat{\sigma}_{AD_Z} + \hat{\sigma}_{BC_Z} + \hat{\sigma}_{BD_Z}, \tag{3.12}$$

where the subscripts indicate the diagram sets involved.

We find that both $\hat{\sigma}_{AC_\gamma}$ and $\hat{\sigma}_{BD_\gamma}$, together with the terms of $\hat{\sigma}_{AC_Z}$ and $\hat{\sigma}_{BD_Z}$, which are proportional to the vector coupling, vanish after integration over event orientations, but they contribute to the forward-backward asymmetry. The $\hat{\sigma}_{AC_Z}$ term proportional to the axial coupling also vanishes upon integration over all event configurations. Finally, after integration over angles the $\hat{\sigma}_{BD_Z}$ term proportional to the axial coupling, being proportional to the Legendre polynomial $P_2(\cos\theta)$, also vanishes. (When introducing cuts, the cancellation is not complete.)

For the nonvanishing graviton-SM interference terms, we get

$$\frac{d^2\hat{\sigma}_{AD_\gamma}}{dx_1dx_2}=-\frac{\alpha^2\kappa^2Q_q^2Q_e^2}{144\pi}\mathrm{Re}\left[\frac{s_3}{s_3-m_{\vec{n}}^2+im_{\vec{n}}\Gamma_{\vec{n}}}\right]X_{AD}(x_1,x_2),$$

$$\frac{d^2\hat{\sigma}_{AD_Z}}{dx_1dx_2}=-\frac{\alpha^2\kappa^2Q_qQ_ev_qv_e}{144\pi}\times\mathrm{Re}\left[\chi^*(\hat{s})\ \frac{s_3}{s_3-m_{\vec{n}}^2+im_{\vec{n}}\Gamma_{\vec{n}}}\right]X_{AD}(x_1,x_2),$$

$$\frac{d^2\hat{\sigma}_{BC_\gamma}}{dx_1dx_2}=-\frac{\alpha^2\kappa^2Q_q^2Q_e^2}{144\pi}\mathrm{Re}\left[\frac{\hat{s}}{\hat{s}-m_{\vec{n}}^2+im_{\vec{n}}\Gamma_{\vec{n}}}\right]X_{BC}(x_1,x_2),\tag{3.13}$$

$$\frac{d^2\hat{\sigma}_{BC_Z}}{dx_1dx_2}=-\frac{\alpha^2\kappa^2Q_qQ_ev_qv_e}{144\pi}\times\mathrm{Re}\left[\chi^*(s_3)\ \frac{\hat{s}}{\hat{s}-m_{\vec{n}}^2+im_{\vec{n}}\Gamma_{\vec{n}}}\right]X_{BC}(x_1,x_2),$$

where $\chi(\hat{s})$ is given by Eq. (3.3), whereas $X_{AD}(x_1,x_2)$ and $X_{BC}(x_1,x_2)$ are given in Appendix A.

To find the contribution from quark-antiquark annihilation to the overall process (1.1), a relation similar to the one given by Eq. (3.4) should be used. However, when there are quark charges or vector and/or axial-vector couplings ($v_q$ or $a_q$) involved, the convolution integrals must be weighted by these factors, as shown in Appendix A.

## IV. BREMSSTRAHLUNG IN THE ADD SCENARIO

In this section we shall consider bremsstrahlung within the ADD scenario [3]. First, we shall present the cross section as a function of invariant mass, and then study the photon distribution (or $k_\perp$ spectrum) of such events.

### A. Total cross section

In the ADD scenario, the coupling of each KK mode to matter is Planck-scale suppressed. However, since the states are very closely spaced, with [7]

$$m_{\vec{n}}^2=\frac{4\pi^2\vec{n}^2}{R^2},\tag{4.1}$$

and $R/2\pi$ the compactification radii, the coherent summation over the many modes leads to effective couplings with strength $1/M_S$, where $M_S$ is the UV cutoff (close to the effective Planck scale).

Explicitly, in this scenario, the graviton coupling is in the $(4+n)$-dimensional theory given by [7]

$$\hat{g}_{MN}=\hat{\eta}_{MN}+\hat{\kappa}\hat{h}_{MN},\quad \hat{\kappa}^2=16\pi G_{\mathrm{N}}^{(4+n)},\tag{4.2}$$

where $G_{\mathrm{N}}^{(4+n)}$ is Newton's constant in $4+n$ dimensions. In 4 dimensions the coupling can be written as

$$\kappa^2=V_n^{-1}\hat{\kappa}^2=16\pi V_n^{-1}\ \ G_{\mathrm{N}}^{(4+n)}=16\pi G_{\mathrm{N}},\tag{4.3}$$

with $V_n$ the volume of the $n$-dimensional compactified space ($V_n=R^n$ for a torus $T^n$) and $G_{\mathrm{N}}$ the 4-dimensional Newton constant.

Summing coherently over all KK modes in a tower, the graviton propagator gets replaced [7]:

$$\frac{1}{\hat{s}-m_{\vec{n}}^2+im_{\vec{n}}\Gamma_{\vec{n}}}\equiv -iD(\hat{s})\to\frac{\hat{s}^{n/2-1}}{\Gamma(n/2)}\ \frac{R^n}{(4\pi)^{n/2}}\ [2I(M_S/\sqrt{\hat{s}})-i\pi],\tag{4.4}$$

with

$$I(M_S/\sqrt{\hat{s}})=\begin{cases}-\sum_{k=1}^{n/2-1}\frac{1}{2k}\left(\frac{M_S}{\sqrt{\hat{s}}}\right)^{2k}-\frac{1}{2}\log\left(\frac{M_S^2}{\hat{s}}-1\right), & n=\text{even},\\ -\sum_{k=1}^{(n-1)/2}\frac{1}{2k-1}\left(\frac{M_S}{\sqrt{\hat{s}}}\right)^{2k-1}+\frac{1}{2}\log\left(\frac{M_S+\sqrt{\hat{s}}}{M_S-\sqrt{\hat{s}}}\right), & n=\text{odd}.\end{cases}\tag{4.5}$$

for $n$ extra dimensions.

Higher order loop effects may be important [22], so these expressions should not be taken too literally. In particular, this applies to the dependence on the number of extra dimensions. In the approach of [5] and [8] this uncertainty, including the $n$ dependence, is absorbed in the cutoff in such a way that $D(\hat{s})$ and $D(s_3)$ [see Eq. (4.4)] are indistinguishable. Here, in order to preserve the qualitative difference between these two propagators, related to final- and initial-state radiation, we shall use the expressions of Eq. (4.5).

Invoking the relation [7]

$$\kappa^2R^n=8\pi(4\pi)^{n/2}\Gamma(n/2)M_S^{-(n+2)}\tag{4.6}$$

between the volume of the extra dimensions, the gravitational coupling and the cutoff scale, the differential cross section can be expressed as

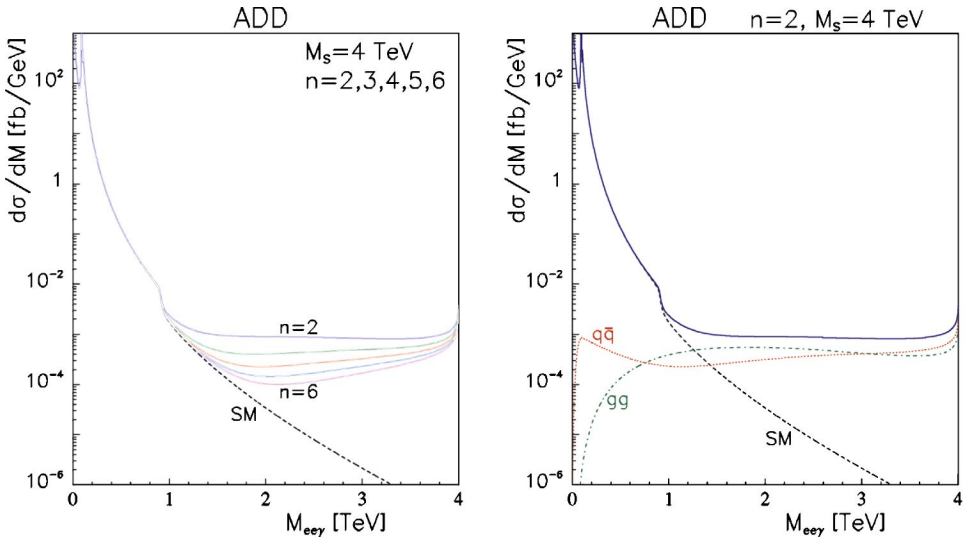


FIG. 3. Cross sections for $pp \to e^+e^-\gamma + X$ at $\sqrt{s}=14$ TeV. Both plots are for the ADD model with $M_S=4$ TeV. We have set the number of extra dimensions (from above) to $n=2,3,4,5$, and 6 for the left panel. The full differential cross section, $d\sigma/d\sqrt{\hat{s}}$ (solid), and the SM background (dashed) are shown in both plots, whereas the $gg$ (dash-dotted) and the $q\bar{q}$ (dotted) contributions to the signal are shown in the right panel for $n=2$.

$$\frac{d^3\sigma}{d\hat{s}dx_1dx_2} = \frac{\alpha s_3}{192 s M_S^4}\left(\frac{s_3}{M_S^2}\right)^n I_{D_\gamma D_\gamma}(\hat{s})[4I^2(M_S/\sqrt{s_3})+\pi^2]X_A(x_1,x_2) + \frac{\alpha Q_e^2 \hat{s}}{120 s M_S^4}\left(\frac{\hat{s}}{M_S^2}\right)^n [3I_{gg}(\hat{s})+2I_{BB}(\hat{s})]$$
$$\times[4I^2(M_S/\sqrt{\hat{s}})+\pi^2]X_B(x_1,x_2) - \frac{\alpha^2}{18 s M_S^2}\left[\left(\frac{s_3}{M_S^2}\right)^{n/2}(2Q_e^2 I_{D_\gamma D_\gamma}(\hat{s})I(M_S/\sqrt{s_3}) + Q_e v_e I_{D_\gamma D_Z}(\hat{s})\right.$$
$$\times \mathrm{Re}\{\chi^*(\hat{s})[2I(M_S/\sqrt{s_3}) - i\pi]\})X_{AD}(x_1,x_2) + \left(\frac{\hat{s}}{M_S^2}\right)^{n/2}(2Q_e^2 I_{D_\gamma D_\gamma}(\hat{s})I(M_S/\sqrt{\hat{s}}) + Q_e v_e I_{D_\gamma D_Z}(\hat{s})$$
$$\left.\times \mathrm{Re}\{\chi^*(s_3)[2I(M_S/\sqrt{\hat{s}}) - i\pi]\})X_{BC}(x_1,x_2)\right] + \frac{d^3\sigma^{(\mathrm{SM})}}{d\hat{s}dx_1dx_2}, \tag{4.7}$$

where $\chi(\hat{s})$ is given by Eq. (3.3) and the convolution integrals are given in Appendix A. The SM background is given by

$$\frac{d^3\sigma^{(\mathrm{SM})}}{d\hat{s}dx_1dx_2} = \frac{\alpha^3}{3 s s_3}\{Q_e^2 I_{C_\gamma C_\gamma}(\hat{s}) + 2Q_e v_e I_{C_\gamma C_Z}(\hat{s})\mathrm{Re}\,\chi(s_3) + (v_e^2+a_e^2)I_{C_Z C_Z}(\hat{s})|\chi(s_3)|^2\}X_C(x_1,x_2) + \frac{16\alpha^3 Q_e^2}{9 s \hat{s}}\{Q_e^2 I_{D_\gamma D_\gamma}(\hat{s})$$
$$+ 2Q_e v_e I_{D_\gamma D_Z}(\hat{s})\mathrm{Re}\,\chi(\hat{s}) + (v_e^2+a_e^2)I_{D_Z D_Z}(\hat{s})|\chi(\hat{s})|^2\}X_D(x_1,x_2) - \frac{8\alpha^3 Q_e a_e}{3 s \hat{s}}\{Q_e I_{C_\gamma D_Z}(\hat{s})$$
$$\times \mathrm{Re}\,\chi(\hat{s}) + Q_e I_{C_Z D_\gamma}(\hat{s})\mathrm{Re}\,\chi(s_3) + 4 v_e I_{C_Z D_Z}(\hat{s})\mathrm{Re}[\chi^*(\hat{s})\chi(s_3)]\}X_{CD}(x_1,x_2). \tag{4.8}$$

In Eq. (4.7), the different contributions are given in the following order: First quark-antiquark annihilation with initial-state radiation (set $A$), then gluon-gluon fusion and quark-antiquark annihilation with final-state radiation (set $B$), various interference terms between graviton exchange and SM amplitudes, and finally the SM background. The origins of the different terms are reflected in the subscripts of the $X$'s.

In Fig. 3 we show the cross section, differential with respect to $\sqrt{\hat{s}}$ (labeled $M_{ee\gamma}$ in the figures), for $M_S=4$ TeV and $n=2,3,4,5$ and 6 (left panel) in the ADD scenario, where we have integrated out the $x_1, x_2$ dependence (see Appendix B). The right panel shows only the $n=2$ curve, with the contributions from gluon-gluon fusion and quark-antiquark annihilation (induced by graviton exchange) also displayed. Note that gluon-gluon fusion is dominant from $\sqrt{\hat{s}} \simeq 1.3$ TeV up to $\sqrt{\hat{s}} \simeq 3$ TeV for this choice of parameters,

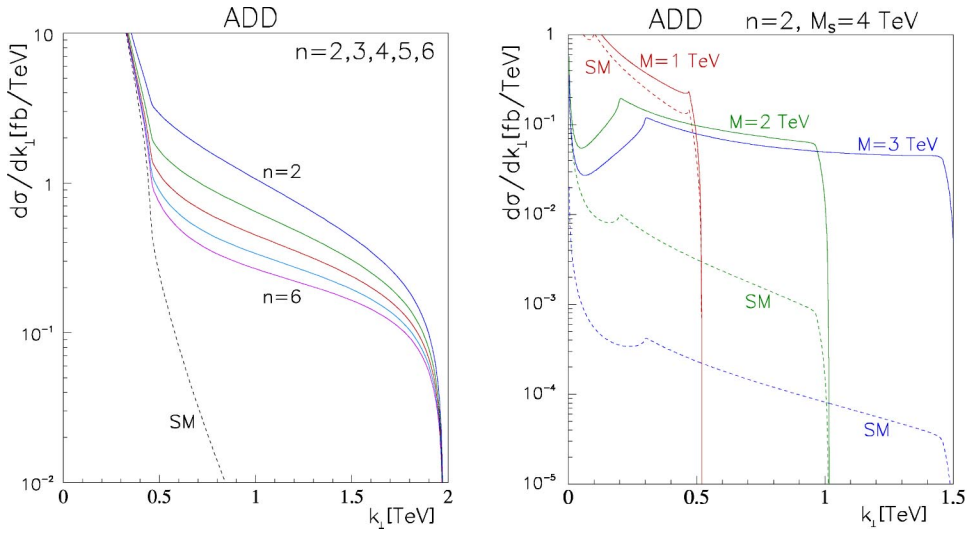


FIG. 4. Photon distributions for the ADD model. Left panel: $d\sigma/dk_\perp$ (solid) with (from above) $n=2,3,4,5,6$ extra dimensions and $M_S=4$ TeV, together with the SM background. Right panel: $d\sigma/dk_\perp$ (solid) for $n=2$ and $M_S=4$ TeV, integrated over 100 GeV bins around $M_{ee\gamma}=M=1,2,3$ TeV, with the corresponding SM backgrounds (dashed).

whereas the quark-antiquark annihilation process takes over at larger invariant masses. Below $\sim 1$ TeV, the background is larger than the signal.

We have integrated over $x_3^{\min} \leqslant x_3 \leqslant 0.5$, subject to the $y$ cuts: $s_1, s_2 \geqslant y\hat{s}$, $s_3 \geqslant y_3 \hat{s}$, where both $y=y_3=0.01$. The minimum invariant mass of the two electrons is controlled by $y_3$. At a scale $\sqrt{\hat{s}}=1$ TeV, the cut of $y=0.01$ corresponds to electron (or photon) energies exceeding 10 GeV. We consider a minimum $x_3$ of 0.1 in these plots. The corresponding resolution is well within that foreseen at the LHC [23]. For the angular cuts, we take the pseudorapidity $|\eta|<2.5$.

Here, and in the remaining figures, we use $\sqrt{s}=14$ TeV, which corresponds to the LHC energy. With an integrated luminosity of 100 fb$^{-1}$ and a bin width of 100 GeV, we might expect a few events per bin at invariant masses above 1 TeV.

Near the $Z$ mass, the cross section has an additional peak (barely visible in the figures) since both the amplitudes with $\hat{s}$ (set $C_Z$) and those with $s_3$ (set $D_Z$) resonate. Also, at $\hat{s} \sim 10 \times m_Z \sim 0.9$ TeV, the cross section has a falloff. In fact, both the second peak and the falloff are related to ''radiative return,'' where the emitted photon has the right energy to make the $Z$ propagator resonate. The peak near $m_Z$ is at the starting point for radiative return, determined by $s_3$ (and hence the lower value for $x_3$), whereas the falloff near 0.9 TeV is related to the end point of the radiative return, given by the upper value of $x_3$, which is $\frac{1}{2}(1-y_3)$.

Close to the cutoff, $M_S$, the cross section increases due to the logarithm in $I(M_S/\sqrt{\hat{s}})$. This is of course an artifact, due to the way the cutoff is treated [22]. Note that the explicit $n$ dependence in Fig. 3 is in the approach of [5,8] absorbed in the cutoff.

Let us now discuss the different terms related to $q\bar{q}$ annihilation. The part of the $q\bar{q}$ annihilation cross section which is related to $X_A$ (initial-state radiation with graviton exchange) is everywhere significantly smaller than the one related to $X_B$ (final-state radiation with graviton exchange), by more than an order of magnitude. This is partly due to the difference in the convolution integrals.

Among the different interference terms, related to $X_{AD}$ and $X_{BC}$, the most important one is that between set $B$ (final-state radiation with graviton exchange) and set $C_\gamma$ (initial-state radiation with photon exchange). For invariant masses below $\sim 1$ TeV, this interference dominates the $q\bar{q}$ part of the signal (but here, it is overwhelmed by the SM background). We note that the SM amplitude does not interfere with the gluon-gluon fusion part of the graviton-mediated amplitude.

### B. Photon distribution

Whereas photons emitted by QED bremsstrahlung tend to be soft and/or collinear with the fermions, the present graviton-induced bremssstrahlung will be more energetic [17], and also emitted at larger angles. A first, qualitative manifestation of this feature is that the transverse momentum spectrum (with respect to the incident beam) will be harder. We shall here make this statement quantitative.

In Sec. IV A, we have integrated the differential cross section over $x_1, x_2$ and $\cos\theta$ to obtain cross sections which are differential with respect to $\sqrt{\hat{s}}$ [see also Eq. (2.4)]. Now we will instead change variables from $(x_1, x_2, \cos\theta)$ via $(x_{12}=x_1-x_2, x_3, \cos\theta)$ to $(x_{12}, k_\perp, k_\parallel)$, where $k_\perp=\omega\sin\theta$ and $k_\parallel=\omega\cos\theta$. Here

$$\sqrt{k_\perp^2+k_\parallel^2}=k=\omega=x_3\sqrt{\hat{s}}, \tag{4.9}$$

with $\omega$ the energy of the photon. After integration over $x_{12}$, $k_\parallel$ and $\sqrt{\hat{s}}$, we get the cross section, differential with respect to $k_\perp$, the photon momentum perpendicular to the beam.

In Fig. 4, left panel, we show $d\sigma/dk_\perp$ for different numbers of extra dimensions, and with $M_S=4$ TeV, where we

have integrated over $\sqrt{\hat{s}}$ up to the cutoff $M_S$. In accordance with Fig. 3, we impose the cuts: $x_3^{\min}\sqrt{\hat{s}} \leqslant k \leqslant \frac{1}{2}(1-y_3)\sqrt{\hat{s}}$. Since the photon should not be too close to the beam axis, we also require $k_\perp \geqslant 100$ GeV. We see that the $k_\perp$ spectrum becomes much harder when extra dimensions are involved.

The right panel of Fig. 4 shows bin-integrated cross sections. Here we have chosen invariant masses of $\sqrt{\hat{s}} = 1,2,3$ TeV, and integrated $d^2\sigma/(dk_\perp d\sqrt{\hat{s}})$ over 100 GeV bins around these values. The peaks at 0.1, 0.2 and 0.3 TeV are also related to cuts on $k$ (or $x_3$). Note that the SM background is very small at higher invariant masses.

## V. BREMSSTRAHLUNG IN THE RS SCENARIO

As in the preceding section we will first present the total cross section, and thereafter the photon distribution, for the Randall-Sundrum scenario [4].

### A. Total cross section

In the RS scenario, the graviton masses are given by [10]

$$m_n = k x_n e^{-k r_c \pi} = \frac{x_n}{x_1} m_1, \tag{5.1}$$

where $x_n$ are roots of the Bessel function[2] of order 1, $J_1(x_n)=0$, $k$ is of the order of the (four-dimensional) Planck scale and $r_c$ the compactification radius of the extra dimension.[3] Since there is only one extra dimension in this scenario, we shall use $m_n$ instead of $m_n^-$ for the mass of the $n$th graviton.

The gravitational coupling is in this model given by [10,12]

$$\kappa = \sqrt{16\pi}\ \frac{x_n}{m_n}\ \frac{k}{\overline{M}_{\rm Pl}} = \sqrt{2}\ \frac{x_1}{m_1}\ \frac{k}{\overline{M}_{\rm Pl}}, \tag{5.2}$$

$$\overline{M}_{\rm Pl} = \frac{M_{\rm Pl}}{\sqrt{8\pi}} = 2.4\times 10^{18}\ \text{GeV}.$$

Here we shall use $m_1$ and $k/\overline{M}_{\rm Pl}$ as the two parameters which specify the model. Note that $0.01 \leqslant k/\overline{M}_{\rm Pl} \leqslant 1$ [10].

The differential cross section can in the RS scenario be expressed as [with the different contributions given in the same order as in Eq. (4.7)]

$$\begin{aligned}\frac{d^3\sigma}{d\hat{s}dx_1dx_2} &= \frac{\alpha s_3}{3072\pi^2 s}\left(\frac{x_1}{m_1}\right)^4\left(\frac{k}{\overline{M}_{\rm Pl}}\right)^4 I_{D_\gamma D_\gamma}(\hat{s})|\mathcal{G}(s_3)|^2 X_A(x_1,x_2) + \frac{\alpha\hat{s}}{1920\pi^2 s}\left(\frac{x_1}{m_1}\right)^4\left(\frac{k}{\overline{M}_{\rm Pl}}\right)^4 Q_e^2[3I_{gg}(\hat{s})+2I_{BB}(\hat{s})] \\ &\times|\mathcal{G}(\hat{s})|^2 X_B(x_1,x_2) - \frac{\alpha^2}{72\pi s}\left(\frac{x_1}{m_1}\right)^2\left(\frac{k}{\overline{M}_{\rm Pl}}\right)^2(\{Q_e^2 I_{D_\gamma D_\gamma}(\hat{s})\,\mathrm{Re}\,\mathcal{G}(s_3) \\ &+ Q_e v_e I_{D_\gamma D_Z}(\hat{s})\,\mathrm{Re}[\chi^*(\hat{s})\mathcal{G}(s_3)]\}X_{AD}(x_1,x_2) + \{Q_e^2 I_{D_\gamma D_\gamma}(\hat{s})\,\mathrm{Re}\,\mathcal{G}(\hat{s}) \\ &+ Q_e v_e I_{D_\gamma D_Z}(\hat{s})\,\mathrm{Re}[\chi^*(s_3)\mathcal{G}(\hat{s})]\}X_{BC}(x_1,x_2)) + \frac{d^3\sigma^{(\rm SM)}}{d\hat{s}dx_1dx_2},\end{aligned} \tag{5.3}$$

where the SM contribution is given by Eq. (4.8). For massive graviton exchange we have introduced the abbreviation

$$\mathcal{G}(\hat{s}) = \sum_n \frac{\hat{s}}{\hat{s}-m_n^2+im_n\Gamma_n} \tag{5.4}$$

with [7,24]

$$\Gamma_n \equiv \frac{\gamma_G}{20\pi}m_n^3\kappa^2 = \frac{\gamma_G}{10\pi}\ x_n^2 m_n\left(\frac{k}{\overline{M}_{\rm Pl}}\right)^2, \tag{5.5}$$

and

$$\gamma_G = 1+\chi_\gamma+\chi_Z+\chi_W+\chi_\ell+\chi_q+\chi_H+\chi_r \tag{5.6}$$

the total graviton width in units of the two-gluon width. Neglecting mass effects, we have [7,24]

$$\begin{aligned}&\chi_\gamma = \frac{1}{8}, \quad \chi_Z = \frac{13}{96}, \quad \chi_W = \frac{13}{48}, \\ &\chi_\ell = \frac{N_\ell}{16}, \quad \chi_q = \frac{N_c N_q}{16}, \quad \chi_H = \chi_r = \frac{1}{48}.\end{aligned} \tag{5.7}$$

Here, $N_\ell = 6$ is the number of leptons, and $N_c N_q = 18$ is the number of quarks weighted with color factors. Note that since we have neglected quark and electron masses, there is no contribution to the cross section from radion exchange,

[2]The first four roots are 3.83, 7.02, 10.17 and 13.32.

[3]To solve the hierarchy problem, $kr_c \sim 12$ is required.

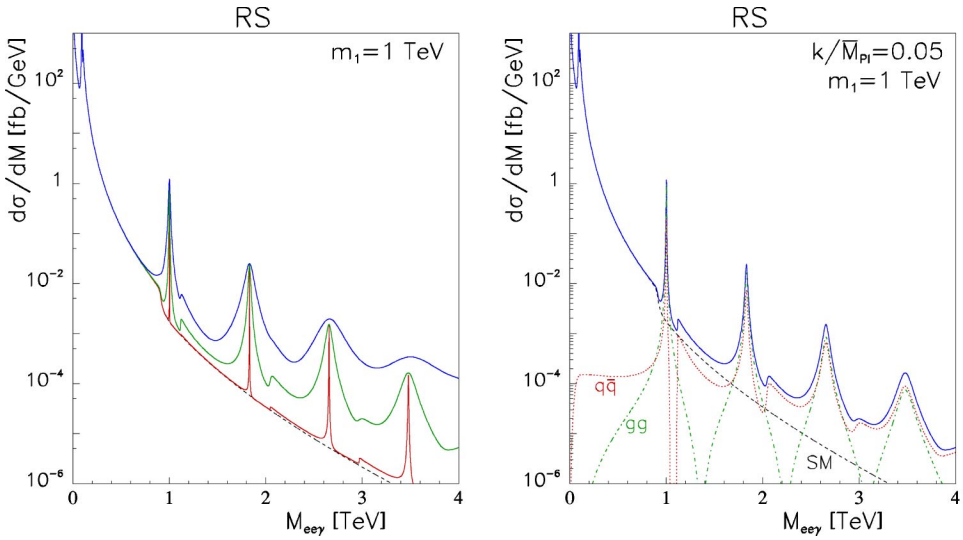


FIG. 5. Differential cross sections for the RS model, with $m_1=1$ TeV. The left panel shows the differential cross section, $d\sigma/d\sqrt{\hat{s}}$ (solid) with (from above) $k/\bar{M}_{\rm Pl}=0.1$, 0.05 and 0.01, and the SM background (dashed). Right panel: the $gg$ (dash dotted) and $q\bar{q}$ (dotted) contributions to the cross section are shown for $k/\bar{M}_{\rm Pl}=0.05$.

since the radion couples to the trace of the energy-momentum tensor. However, it contributes slightly to $\Gamma_n$ through Eq. (5.5).

We display the RS scenario cross section, differential with respect to $\sqrt{\hat{s}}$ [see Eq. (5.3)], in Fig. 5. In the left panel, we have summed over KK states, and chosen the first graviton resonance at $m_1=1$ TeV, with $k/\bar{M}_{\rm Pl}$ set to 0.1, 0.05 and 0.01 (from above). In the right panel, we show the different contributions ($gg$ and $q\bar{q}$) to the cross section (for $k/\bar{M}_{\rm Pl}=0.05$) induced by graviton exchange. The cuts are the same as in the ADD case.

As we mentioned above, the integration over $s_3$ (or $x_3$) will smear out the contribution from initial-state radiation. For invariant masses greater than

$$\sqrt{\hat{s}}=\frac{m_1}{\sqrt{1-2x_3^{\rm min}}}\simeq 1.1m_1, \tag{5.8}$$

$s_3^{\rm max}$ will always be greater than $m_1$, and radiative return to the first graviton resonance gives a small peak at this value, Eq. (5.8), and similarly for the higher resonances. In fact, these secondary peaks are mainly due to the term involving $X_A$ (initial-state bremsstrahlung with graviton exchange), which gives no visible effect in the ADD case.

Similar to the ADD case, for invariant masses below $\sim 1$ TeV, it is the interference between set $B$ and set $C_\gamma$ which dominates the $q\bar{q}$ signal (dotted). Between the peak at 1 TeV and the secondary peak next to it (due to radiative return) this interference term becomes negative, resulting in a dip in the total cross section. In fact, the total $q\bar{q}$ signal (graviton exchange plus its interference with the SM amplitude) is negative in some small region of invariant mass. However, these structures depend on details of the cuts imposed.

It should be noted that the third and fourth peaks should be somewhat reduced since we have not taken into account that these gravitons can decay into the first KK resonance. Self-interactions of the gravitons were considered in [25], where a BR of about 15% was found for the $G_3\to G_1G_1$ decay.

By comparing Figs. 3 and 5, we see that the difference between the two scenarios is striking, with extremely narrow and widely separated resonances in the RS case, compared to the continuum in the ADD case. Note that according to our expressions, the $k/\bar{M}_{\rm Pl}$ dependence cancels at the resonance. A single peak should therefore have a height which is independent of $k/\bar{M}_{\rm Pl}$, but at very high invariant masses we see that the $k/\bar{M}_{\rm Pl}=0.1$ peak is higher than the other peaks, and also slightly shifted. This is mainly due to interference with and overlap of the neighboring peaks which are very broad.

Since the cross sections for graviton-induced bremsstrahlung are much lower than for the corresponding two-body final state, an important question is, however, if there is any chance of seeing these resonances in the experiments. To give an order of magnitude estimate of the number of events to expect from these narrow peaks, we have integrated the differential cross sections given in Fig. 5 over bins in $M_{ee\gamma}$. In the upper left panel of Fig. 6 we integrate over $\sqrt{\hat{s}}$, starting from $\sqrt{\hat{s}}=M_{ee\gamma}^{\rm min}$. The different curves correspond to $k/\bar{M}_{\rm Pl}=0.1$, 0.05 and 0.01 (from above) for $m_1=0.5$ (solid), 1 (dotted) and 1.5 TeV (dash-dotted). This should be compared to the SM background (dashed) which is also shown. In the remaining panels of Fig. 6 we have integrated over 100 GeV bins for the same choice of $k/\bar{M}_{\rm Pl}$, for $m_1=0.5$, 1.0 and 1.5 TeV.

We see that for these parameters it should be possible to resolve at least the first peak, and in most cases several peaks are visible. We emphasize that this is not a simulation, but

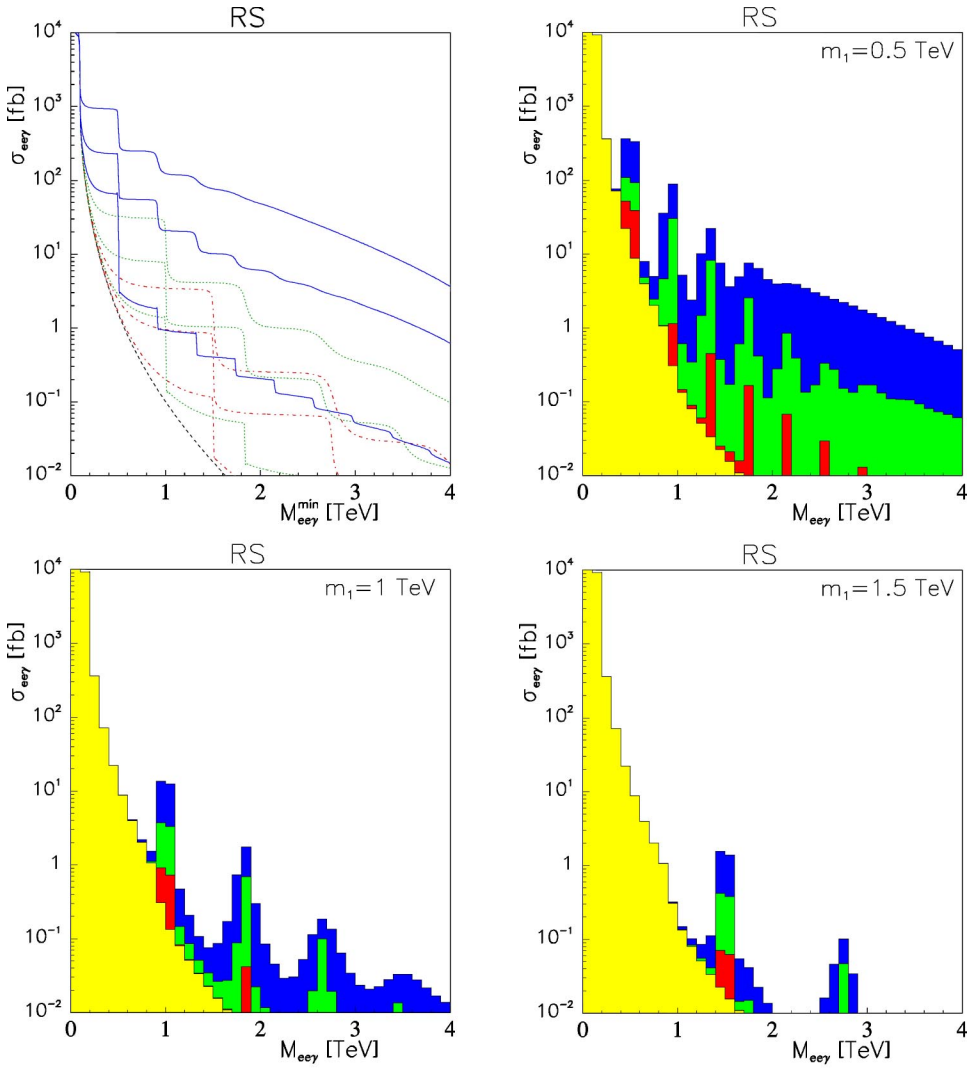


FIG. 6. Integrated cross sections for the RS scenario. In the upper left panel we have integrated the cross sections in Fig. 5 over $\sqrt{\hat{s}}$ for $\sqrt{\hat{s}} \geqslant M_{ee\gamma}^{\min}$. The choice of parameters is $k/\bar{M}_{\rm Pl}=0.1$, 0.05 and 0.01 (from above) for $m_1=0.5$ (solid), 1 (dotted) and 1.5 TeV (dash-dotted). The SM background (dashed) is also shown. The other three panels show the corresponding result of integrating over 100 GeV bins, with $m_1=0.5$ (upper right), $m_1=1$ (lower left) and $m_1=1.5$ TeV (lower right).

these plots should provide an indication of the number of events that correspond to these narrow peaks.

### B. Photon distribution

The photon distribution is also in the RS case harder than the SM background. In the left panel of Fig. 7 we show $d\sigma/dk_\perp$, having integrated over $\sqrt{\hat{s}}$. The steps occur when $k_\perp$ equals half the invariant mass of a RS graviton, since this limits the photon momentum.

The right panel of Fig. 7 again shows bin-integrated cross sections, but now we have chosen 100 GeV bins around the first three resonances, $\sqrt{\hat{s}}=m_1$, $m_2$, $m_3$, since this is where most of the events will occur. We see a similar behavior as in the ADD scenario.

## VI. CONCLUDING REMARKS

In summary, we have discussed photon bremsstrahlung induced by the exchange of massive gravitons at the LHC. Both the ADD and the RS scenarios have been considered. We found that three-body final states are likely to be detectable, and could be a valuable supplement to the two-body final states, for the purpose of detecting the effects from massive gravitons related to extra dimensions (if such exist). These configurations, of a hard photon associated with an electron–positron (or muon) pair in the opposite direction, should provide a striking signature at the LHC. Furthermore, the photon has a harder distribution in transverse momentum than the SM background.

We have here focused on bremsstrahlung at the LHC. At the Fermilab, the phenomenology will be rather different. Because of the lower energy, and because of the different initial state, quark-antiquark annihilation will be much more important, relative to the gluon-gluon initial state. Furthermore, there will in $p\bar{p}$ collisions be additional contributions to the forward-backward asymmetries, beyond those of the SM. Such asymmetries will be induced by interference be-

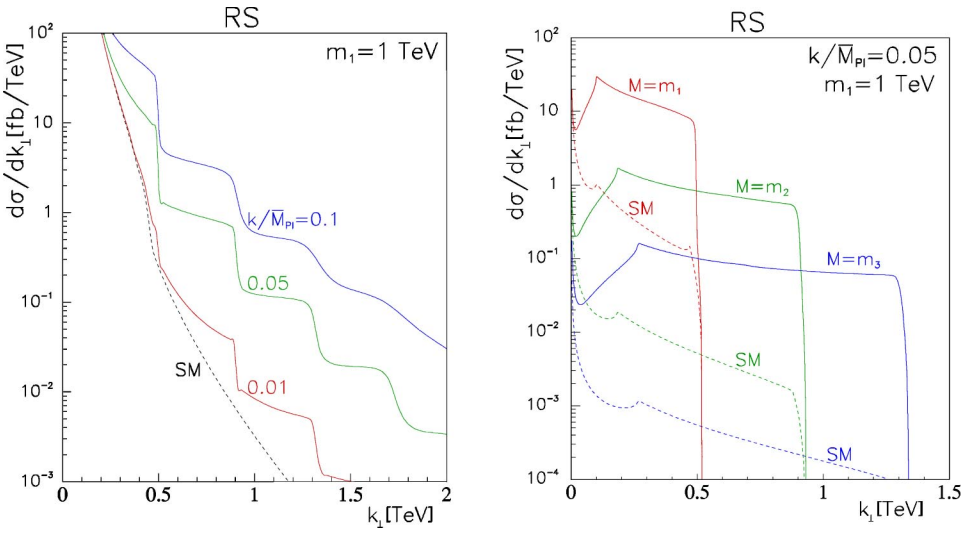


FIG. 7. Photon distributions for the RS model. Left panel: $d\sigma/dk_\perp$ (solid) with (from above) $k/\bar{M}_{\rm Pl}=0.1$, 0.05, 0.01, $m_1=1$ TeV and the SM background (dashed). Right panel: $d\sigma/dk_\perp$ (solid) with $m_1=1$ TeV and $k/\bar{M}_{\rm Pl}=0.05$, integrated over 100 GeV bins around the first three resonances, with corresponding SM backgrounds.

tween the $C$-odd exchange of a photon or a $Z$, and the $C$-even exchange of a graviton, as well as by the interference between graviton-exchange with initial-state radiation and graviton-exchange with final-state radiation. This effect, which is washed out at the LHC because of the symmetry of the initial state, is of course present also for $e^+e^-\to f\bar{f}$ [8], and will have an analogue in the three-body final states. We hope to discuss this effect elsewhere.

## ACKNOWLEDGMENTS

It is a pleasure to thank Hans Bijnens, John Ellis, Gian Giudice, JoAnne Hewett, and, in particular, Paolo di Vecchia for very useful discussions. This research has been supported by the Research Council of Norway and by NORDITA. The work of N.Ö. was supported in part by the Robert A. Welch Foundation.

## APPENDIX A: CONVOLUTION INTEGRALS AND EVENT SHAPES

In this appendix we define the convolution integrals and the event shapes used in our expressions. First, the basic convolution integrals are

$$I_{gg}(\hat{s})=\int_{-Y}^{Y}dy f_g\left(\sqrt{\frac{\hat{s}}{s}}\,e^{y}\right)f_g\left(\sqrt{\frac{\hat{s}}{s}}\,e^{-y}\right),$$
$$I_{q\bar{q}}(\hat{s})=\int_{-Y}^{Y}dy f_q\left(\sqrt{\frac{\hat{s}}{s}}\,e^{y}\right)f_{\bar{q}}\left(\sqrt{\frac{\hat{s}}{s}}\,e^{-y}\right), \tag{A1}$$

with $Y=\frac{1}{2}\log(s/\hat{s})$, and where in the latter case, a specific quark flavor $q$ is considered. The quark convolution integrals enter in the cross section weighted with different coupling constants and summed over quark flavors:

$$I_{BB}(\hat{s})=2\sum_q I_{q\bar{q}}(\hat{s}),\quad I_{C_\gamma C_\gamma}(\hat{s})=2\sum_q Q_q^4 I_{q\bar{q}}(\hat{s}),$$
$$I_{C_\gamma C_Z}(\hat{s})=2\sum_q Q_q^3 v_q I_{q\bar{q}}(\hat{s}),$$
$$I_{C_Z C_Z}(\hat{s})=2\sum_q Q_q^2(v_q^2+a_q^2) I_{q\bar{q}}(\hat{s}),$$
$$I_{D_\gamma D_\gamma}(\hat{s})=2\sum_q Q_q^2 I_{q\bar{q}}(\hat{s}),\quad I_{D_\gamma D_Z}(\hat{s})=2\sum_q Q_q v_q I_{q\bar{q}}(\hat{s}), \tag{A2}$$
$$I_{D_Z D_Z}(\hat{s})=2\sum_q (v_q^2+a_q^2) I_{q\bar{q}}(\hat{s}),$$
$$I_{C_\gamma D_Z}(\hat{s})=I_{C_Z D_\gamma}(\hat{s})=2\sum_q Q_q^2 a_q I_{q\bar{q}}(\hat{s}),$$
$$I_{C_Z D_Z}(\hat{s})=2\sum_q Q_q v_q a_q I_{q\bar{q}}(\hat{s}).$$

These integrals are labeled according to the sets of Feynman diagrams which are associated with the couplings involved. Integrals involving SM couplings also enter in interference terms involving graviton exchange. Note the factor of two in the $q\bar{q}$ convolutions, which accounts for the fact that at a $pp$ collider, either beam can provide the quark or the antiquark. All convolution integrals have been evaluated with CTEQ5 parton distribution functions [26].

The event shape distributions of the different contributions to the cross section can be expressed in terms of $x_1$, $x_2$ and $x_3=1-x_1-x_2$. It is convenient to express these quantities in terms of the abbreviations:

$$
\begin{aligned}
z_a &= 8x_3^4 - 12x_3^2 + 12x_3 - 3, \\
z_b &= 3x_3^2(1-2x_3)(2x_3^2 - 2x_3 + 1), \\
z_c &= 2x_3^4(x_1+x_2)^2(4x_3^2 - 2x_3 + 1), \\
z_d &= 6(1-2x_3)(4x_3^2 - 10x_3 + 5), \\
z_e &= 9x_3^2(1-2x_3)(2x_3^2 - 6x_3 + 3), \\
z_f &= 8x_3^4 - 80x_3^3 + 180x_3^2 - 140x_3 + 35,
\end{aligned}
\tag{A3}
$$

$$
\begin{aligned}
z_g &= 2x_3^2 + 2x_3 - 1, \\
z_h &= 2x_3^2 - 6x_3 + 3, \\
z_i &= 8x_3^2 - 4x_3 + 3, \\
z_j &= 8x_3^2 - 10x_3 + 3, \\
z_k &= 12x_3^2 - 8x_3 + 3.
\end{aligned}
$$

We first give the expression for initial-state radiation, expressed as an integral over $\cos\theta$,

$$
X_A(x_1,x_2) = \int d(\cos\theta)\, \frac{a_0(x_1,x_2) + a_2(x_1,x_2)\cos^2\theta + a_4(x_1,x_2)\cos^4\theta}{x_3^6(1-2x_3)(1-\cos^2\theta)}, \tag{A4}
$$

with

$$
\begin{aligned}
a_0(x_1,x_2) &= -(x_1-x_2)^4 z_a - (x_1-x_2)^2 z_b + z_c, \\
a_2(x_1,x_2) &= -(x_1-x_2)^4 z_d + (x_1-x_2)^2 z_e - x_3^2 z_b, \\
a_4(x_1,x_2) &= (x_1-x_2)^4 z_f - (x_1-x_2)^2 x_3^2 z_d - x_3^4 z_a.
\end{aligned}
\tag{A5}
$$

For the initial-state SM background terms we have

$$
X_C(x_1,x_2) = \int d(\cos\theta)\ \frac{c_0(x_1,x_2) + c_2(x_1,x_2)\cos^2\theta}{x_3^4(1-\cos^2\theta)}, \tag{A6}
$$

with

$$
\begin{aligned}
c_0(x_1,x_2) &= (x_1-x_2)^2 z_g + x_3^2 z_h, \\
c_2(x_1,x_2) &= (x_1-x_2)^2 z_h + x_3^2 z_g.
\end{aligned}
\tag{A7}
$$

We impose a cut on the photon emission angle $\theta$, given by $|\eta| < 2.5$, to render the integrals $X_A$ and $X_C$ finite.

For the remaining quantities, the integration over $\cos\theta$ is trivial, and one finds

$$
X_B(x_1,x_2) = X_D(x_1,x_2) + \frac{8(x_1^2+x_2^2)}{1-2x_3},
$$

$$
X_D(x_1,x_2) = \frac{2(x_1^2+x_2^2)}{(1-2x_1)(1-2x_2)},
$$

$$
X_{AD}(x_1,x_2) = (1-2x_3)\frac{(x_1-x_2)^2 z_i + x_3^2 z_j}{x_3^4}, \tag{A8}
$$

$$
X_{BC}(x_1,x_2) = \frac{(x_1-x_2)^2 z_k + x_3^2(3-2x_3)}{x_3^4(1-2x_3)},
$$

$$
X_{CD}(x_1,x_2) = \frac{x_1+x_2}{x_3^2}.
$$

## APPENDIX B: DEFINITION OF *y* CUTS

Here we shall define quantities where the $x_1, x_2$ dependence (which determines event shapes) in the cross sections is integrated out. When we carry out these integrations, we will impose $y$ cuts. In the case of gluon-gluon fusion, we define

$$
S^{(G)}_{gg\to ee\gamma} = \int \int_{s_i > y\hat{s}} dx_1 dx_2\ \ X_B(x_1,x_2). \tag{B1}
$$

These $y$ cuts will remove IR soft and collinear events where the photon has little energy, or its direction is close to that of an electron. The cut $y_3$, which could be milder, will remove events where the two electrons are close.

In the case of quark-antiquark annihilation, the approach is the same, so we will not write out the integrals here. However, for terms involving initial-state radiation and related interference terms which depend on $s_3 = (1-2x_3)\hat{s}$, all factors involving $s_3$ must be part of the integrand, since $x_1$ and $x_2$ are related to $x_3$.

[1] I. Antoniadis, Phys. Lett. B **246**, 377 (1990).
[2] K. Akama, Lect. Notes Phys. **176**, 267 (1982); V.A. Rubakov and M.E. Shaposhnikov, Phys. Lett. **125B**, 136 (1983); E. Witten, Nucl. Phys. **B443**, 85 (1995); P. Hořava and E. Witten,

*ibid.* **B460**, 506 (1996); P. Hořava and E. Witten, *ibid.* **B475**, 94 (1996).
[3] N. Arkani-Hamed, S. Dimopoulos, and G. Dvali, Phys. Lett. B **429**, 263 (1998); Phys. Rev. D **59**, 086004 (1999).
[4] L. Randall and R. Sundrum, Phys. Rev. Lett. **83**, 3370 (1999); **83**, 4690 (1999).
[5] G.F. Giudice, R. Rattazzi, and J.D. Wells, Nucl. Phys. **B544**, 3 (1999).
[6] E.A. Mirabelli, M. Perelstein, and M.E. Peskin, Phys. Rev. Lett. **82**, 2236 (1999); S. Cullen, M. Perelstein, and M.E. Peskin, Phys. Rev. D **62**, 055012 (2000).
[7] T. Han, J.D. Lykken, and R. Zhang, Phys. Rev. D **59**, 105006 (1999).
[8] J.L. Hewett, Phys. Rev. Lett. **82**, 4765 (1999).
[9] K. Cheung, Phys. Rev. D **61**, 015005 (2000).
[10] H. Davoudiasl, J.L. Hewett, and T.G. Rizzo, Phys. Rev. Lett. **84**, 2080 (2000).
[11] H. Davoudiasl, J.L. Hewett, and T.G. Rizzo, Phys. Rev. D **63**, 075004 (2001).
[12] J. Bijnens, P. Eerola, M. Maul, A. Månsson, and T. Sjöstrand, Phys. Lett. B **503**, 341 (2001).
[13] J. Hewett and M. Spiropulu, hep-ph/0205106.
[14] G. Landsberg, hep-ex/0105039.
[15] CDF Collaboration, D. Acosta *et al.*, Phys. Rev. Lett. **89**, 281801 (2002).
[16] S. Hannestad and G. Raffelt, Phys. Rev. Lett. **87**, 051301 (2001); **88**, 071301 (2002); Y. Uehara, Mod. Phys. Lett. A **17**, 1551 (2002).
[17] E. Dvergsnes, P. Osland, and N. Öztürk, in *Proceedings of the XVIth International Workshop on High Energy Physics and Quantum Field Theory* (QFTHEP'01, Moscow, 2001), edited by M.N. Dubinin and V.I. Savrin (Moscow State University, Moscow, 2001), p. 54, hep-ph/0108029.
[18] E. Gabrielli and B. Mele, Nucl. Phys. **B647**, 319 (2002).
[19] H.A. Olsen, P. Osland, and I. Øverbø, Nucl. Phys. **B171**, 209 (1980).
[20] F.A. Berends and R. Kleiss, Nucl. Phys. **B177**, 237 (1981).
[21] F.A. Berends, R. Kleiss, and S. Jadach, Nucl. Phys. **B202**, 63 (1982).
[22] R. Contino, L. Pilo, R. Rattazzi, and A. Strumia, J. High Energy Phys. **06**, 005 (2001).
[23] See, e.g., ATLAS Detector and Physics Performance Technical Design Report, CERN-LHCC-99-14 and CERN-LHCC-99-15, (1999) http://atlas.web.cern.ch/Atlas/GROUPS/PHYSICS/TDR/access.html, G. L. Bayatian *et al.*, CMS Technical Proposal, CERN-LHCC-94-38 (1994), http://cmsinfo.cern.ch/TP/TP.html.
[24] B.C. Allanach, K. Odagiri, M.A. Parker, and B.R. Webber, J. High Energy Phys. **09**, 019 (2000).
[25] H. Davoudiasl and T.G. Rizzo, Phys. Lett. B **512**, 100 (2001).
[26] CTEQ Collaboration, H.L. Lai *et al.*, Eur. Phys. J. C **12**, 375 (2000).